Remote sensing of cirrus cloud parameters using advanced very-high-resolution radiometer 3.7- and 10.9-μm channels

S. C. Ou, K. N. Liou, W. M. Gooch, and Y. Takano

We develop a retrieval scheme by using advanced very-high-resolution radiometer (AVHRR) 3.7- and 10.9-μm data to compute simultaneously the temperature, optical depth, and mean effective ice-crystal size for cirrus clouds. The methodology involves the numerical solution of a set of nonlinear algebraic equations derived from the theory of radiative transfer. The solution requires the correlation of emissivities of two channels in terms of the effective extinction ratio. The dependence of this ratio on ice-crystal size distribution is examined by using an adding-doubling radiative transfer program. Investigation of the effects of cirrus parameters on upwelling radiances reveals that the brightness-temperature difference between the two channels becomes larger for colder cirrus and smaller ice-crystal sizes. We apply the current retrieval scheme to satellite data collected at 0930 UTC, 28 October 1986, over the region of the First International Satellite Cloud Climatology Project Regional Experiment Cirrus Intensive Field Observation. We select the data over an area (~44° N, 92° W) near Fort McCoy, Wisconsin, for analysis. The retrieved cirrus heights compare reasonably well with lidar measurements taken at Fort McCoy 2 h after a satellite overpass at the target region. The retrieved mean effective crystal size is close to that derived from *in situ* aircraft measurements over Madison, Wisconsin, six hours after a satellite overpass.

1. Introduction

Cirrus clouds are global in nature and occur primarily in the upper troposphere and lower stratosphere. These clouds are composed almost entirely of ice crystals. Information on cirrus cloud parameters is critically important to the development of cirrus cloud forecast models, the upgrading of real-time global cloud analysis, and the investigation of cloud feedbacks in global climate change.[1]

In recent years, data from multichannel imagery sources, particularly the advanced very-high-resolution radiometer (AVHRR) on board National Oceanic and Atmospheric Administration (NOAA) operational satellites, have been available for the retrieval of cloud parameters. Verification of the retrieved results has also become possible because we now have access to measurements by instruments on board aircraft, ground-based lidar, and rawinsonde that were used during the First International Satellite Cloud Climatology Project Regional Experiment (FIRE) Cirrus Intensive Field Observation (IFO) over Wisconsin during October–November 1986.

Numerous methods have been proposed to infer cirrus cloud parameters by using satellite infrared (IR) imaging channels. Liou[2] proposed a method based on four spectral bands in the 10-μm window region to determine the cloud thickness and emissivity. Szejwach[3] developed a technique based on the European Meterological Satellite channels in the 6.5-μm H_2O band and the 10-μm window band to determine cirrus temperature and emissivity. In a similar approach, Pollinger and Wendling[4] used the 6.3- and 11.0-μm spectral bands to infer the height of optically thin ice clouds. Huang and Liou[5] described a dual-channel and dual-scanning angle technique for determining cirrus optical depth and temperature by using the 3.7- and 10.9-μm spectral channels of an AVHRR. A general retrieval program for cloud parameters by using AVHRR channels has also been discussed by Arking and Childs.[6] More recently, Liou *et al.*[7] developed a physical retrieval method to infer the temperature and optical depth of tropical cirrus anvils by using the data of the dual-channel

S. C. Ou and W. M. Gooch are with Liou and Associates, Salt Lake City, Utah 84124; K. N. Liou and Y. Takano are with the Center for Atmospheric and Remote Sounding Studies/Department of Meteorology, University of Utah, Salt Lake City, Utah 84112.

Received 27 December 1991.
0003-6935/93/122171-10$05.00/0.

(6.5- and 10.5-μm), downward-viewing, narrow-field-of-view radiometers on board NASA ER-2. In that work, an iterative numerical scheme was developed to solve the resultant nonlinear algebraic equations. In addition, the effects of scattering by nonspherical ice crystals on cirrus emissivities have been taken into account in radiative transfer calculations. The effects of nonspherical particles on the radiances over cirrus clouds have also been examined by Ackerman and Smith[8] and Kinne *et al.*[9]

Another approach to inferring cirrus parameters utilizes the properties of the brightness-temperature difference (BTD) between AVHRR IR channels. Inoue[10] showed that the cirrus cloud top temperature and the IR effective emissivity may be inferred from BTD values between AVHRR channel (Ch.) 4, 10.9 μm, and Ch. 5, 12 μm. He also showed that positive BTD values for these two channels are always associated with semitransparent cirrus clouds and that the BTD is sensitive to cirrus radiative and microphysical properties. Wu[11] investigated the dependence of the BTD between AVHRR 10.9- and 12-μm channels on the cirrus particle size and temperature. d'Entremont *et al.*[12] derived optical depths and altitudes of cirrus clouds over the FIRE–IFO region in the early morning of 28 October 1986 by using AVHRR Chs. 3, 4, and 5 BTD's and comparing these with calculated and observed values for clear areas. Stone *et al.*[13] examined the BTD between the Geostationary Operational Environmental Satellite 3.9- and 12.7-μm channels as a function of optical depth and microphysics and showed that the 3.9-μm radiances are sensitive to cirrus microphysical properties. However, they developed a retrieval method to compute the cirrus optical depth by using only the AVHRR 10.8-μm channel data. This method requires the estimate of both cloud base radiance and cloud emission by using radiosonde and lidar data. Cloud temperature and ice-crystal size are not determined from the retrieval. In all the preceding investigations that used the BTD method, the absorption and the scattering properties of nonspherical ice crystals have not been accounted for in the retrieval program.

In this paper we have developed a physical retrieval scheme to infer cirrus cloud parameters from the theory of radiative transfer and by using the AVHRR 3.7- and 10.9-μm channels. Analysis has been focused on the sensitivity of channel radiances to the height and mean effective crystal size of cirrus clouds. Moreover we illustrate that the BTD is a good indicator for the presence of cirrus clouds, and we apply the retrieval scheme to the AVHRR satellite data collected at 0930 UTC, 28 October 1986, over the FIRE-IFO region. Section 2 describes the retrieval algorithm. Section 3 presents the results of sensitivity studies and discusses the implications of using the BTD to identify the presence of cirrus clouds. In Section 4 we demonstrate the applicability of the retrieval algorithm to real satellite data. Finally, conclusions are given in Section 5.

2. Retrieval of Cirrus Cloud Parameters

The retrieval program for deriving cirrus temperature, mean effective crystal size, and optical depth from upwelling radiances of AVHRR cloud detection channels follows the principles of the dual-IR-channel technique presented in Liou *et al.*[7] The AVHRR 3.7-μm (Ch. 3) and 10.9-μm (Ch. 4) radiances have been selected for the development. A major advantage of using these two channels for cirrus retrieval is that the radiances of these spectral regions are affected relatively little by the presence of water vapor. However, the Ch. 3 radiances for local daytime contain solar radiation that is reflected by the Earth-atmosphere system. Thus the algorithm described in this section is applicable to cirrus retrieval for local nighttime conditions. It may be used for daytime cirrus retrieval if the solar contamination in the Ch. 3 radiance is removed by an adequate method.

From the theory of radiative transfer, we may express the upwelling radiances at the top of the atmosphere for Ch. 3 and Ch. 4 over a cirrus cloudy atmosphere in terms of the cirrus mean temperature T_c and emissivities $\epsilon_{3,4}$, as follows:

$$R_3 \cong R_{a3}(1 - \epsilon_3) + \epsilon_3 B_3(T_c), \tag{1a}$$

$$R_4 \cong R_{a4}(1 - \epsilon_4) + \epsilon_4 B_4(T_c), \tag{1b}$$

where R_{a3} and R_{a4} denote the upwelling radiances reaching the cloud base for the two spectral bands and $B_3(T_c)$ and $B_4(T_c)$ are the respective Planck intensities at T_c. The first terms on the right-hand side of expressions (1a) and (1b) represent the contribution of the transmitted radiance from below the cloud. The second terms denote the emission contribution from the cloud itself. The emission by water vapor above the cirrus cloud has been neglected. The effects of cloud reflectivity, which are generally less than 3% of the incident radiance based on exact radiative transfer calculations, have also been neglected.

In order to solve expressions (1) for T_c and $\epsilon_{3,4}$ numerically, we need to relate ϵ_3 and ϵ_4 and $B_3(T_c)$ and $B_4(T_c)$. The clear radiances $R_{a3,4}$ must also be known. First we compute the Planck intensities $B_3(T_c)$ and $B_4(T_c)$, taking into account the filter functions of both channels. A look-up table for both $B_3(T_c)$ and $B_4(T_c)$ in 1-K intervals is constructed by using a range of T_c from 150 to 300 K. Values in the look-up table are then fitted to a third-degree polynomial based on a least-squares regression method:

$$B_3(T_c) = \sum_{n=0}^{3} a_n [B_4(T_c)]^n = f(B_4). \tag{2}$$

The resulting coefficients are $a_0 = 2.6327 \times 10^{-4}$, $a_1 = -1.063 \times 10^{-4}$, $a_2 = 8.2976 \times 10^{-6}$, and $a_3 = 3.7311 \times 10^{-7}$. Errors in the fitted polynomial are less than 1%.

Second, we investigate the relationship between the emissivities for the two channels. From radia-

tive transfer calculations and following the approach proposed by Liou *et al.*[7], we may parameterize cirrus emissivities at the 3.7- and 10.9-μm wavelengths in terms of visible optical depths τ in the form

$$\epsilon_3 = 1 - \exp(-k_3\tau), \tag{3a}$$

$$\epsilon_4 = 1 - \exp(-k_4\tau). \tag{3b}$$

The exponential terms represent the effective transmissivities. The parameters k_3 and k_4 account for multiple scattering within cirrus clouds and for the difference between visible and IR extinction coefficients. Both k_3 and k_4 are smaller than 1 because the effect of multiple scattering increases transmission. Thus the products $k_3\tau$ and $k_4\tau$ may be considered as effective optical depths, which are the optical depths that would yield the same emissivity values for nonscattering conditions at the 3.7- and 10.9-μm wavelengths. By eliminating τ from Eqs. (3) we obtain

$$(1 - \epsilon_3)^{1/k_3} = (1 - \epsilon_4)^{1/k_4}. \tag{4}$$

Equation (4) relates ϵ_3 with ϵ_4 directly. A further combination of expressions (1) and Eq. (4) leads to

$$\left[\frac{R_3 - B_3(T_c)}{R_{a3} - B_3(T_c)}\right]^{1/k_3} = \left[\frac{R_4 - B_4(T_c)}{R_{a4} - B_4(T_c)}\right]^{1/k_4}. \tag{5}$$

Substitution of Eq. (2) into Eq. (5) results in a nonlinear algebraic equation, with $B_4(T_c)$ as the only unknown:

$$\frac{R_4 - B_4(T_c)}{R_{a4} - B_4(T_c)} - \left\{\frac{R_3 - f[B_4(T_c)]}{R_{a3} - f[B_4(T_c)]}\right\}^{k_4/k_3} = 0. \tag{6}$$

We investigate the dependence of these parameters on the optical depth based on radiative transfer calculations by using two cirrus cloud types involving small cirrostratus (Cs) and large cirrus uncinus (Ci) ice crystals. A reasonable range of optical depth for Cs and Ci is shown in Table 1. In both cases, the variations of k_4 and k_3 are less than ~2%. As a good approximation, we may take k_4 and k_3 as independent of the optical depth. This will eliminate the complexity of retrieving the optical depth from satellite measurements.

The ratio k_4/k_3 in Eq. (6) can be considered to be the effective extinction ratio, which, as is shown below, is primarily dependent on ice-crystal size distribution. We have analyzed 12 size distribution functions of cirrus clouds that were obtained from the data presented in Heymsfield and Platt,[14] Takano and Liou,[15] and recently obtained from the FIRE–IFO. We first define a mean effective width (or size) to represent ice-crystal size distribution in the form

$$D_e = \int D \cdot LDn(L)\mathrm{d}L \Big/ \int LDn(L)\mathrm{d}L, \tag{7}$$

where D and L denote the width and the maximum dimension of a nonspherical ice crystal, respectively, and $n(L)$ is the size distribution in terms of L. The rationale for defining D_e to represent ice-crystal size distribution is that the scattering of light is related to the geometric cross section, which is proportional to LD. Light scattering and absorption programs developed by Takano and Liou[15] for hexagonal ice crystals and radiative transfer programs developed by Takano and Liou[16] and Liou *et al.*[17] have been used to compute cirrus emissivity as a function of D_e.

Figure 1 shows the dependence of k_4/k_3 on D_e based on the 12 measured size distributions mentioned above. Generally k_4/k_3 decreases as D_e increases. For a small D_e (~20 μm), k_4/k_3 ~ 3, which is much larger than 1. This is primarily because the single-scattering albedo is larger for the 3.7-μm wavelength (~0.79) than that for the 10.9-μm wavelength (~0.41), which implies that more scattering is associated with the former wavelength. For $D_e > 100$ μm, k_4/k_3 approaches 1 for the following reasons. First, the extinction coefficients are approximately the same for the two wavelengths because of large-size parameters in which the geometric optics limit is valid. Second, the single-scattering albedos are also approximately the same for these wavelengths because substantial absorption occurs within large ice crystals so that only the diffracted and externally reflected light contributes to the scattering processes. We have carried out a second-degree polynomial least-

Table 1. Values of k_4 and k_3 as Functions of the Visible Optical Depth τ

Cirrostratus (Cs)			Cirrus Uncinus (Ci)		
τ	k_3	k_4	τ	k_3	k_4
0.05	0.290	0.516	0.2	0.416	0.497
0.10	0.292	0.517	0.5	0.419	0.498
0.20	0.295	0.518	1.0	0.422	0.499
0.50	0.302	0.520	2.0	0.426	0.502
1.00	0.308	0.522	5.0	0.428	0.504

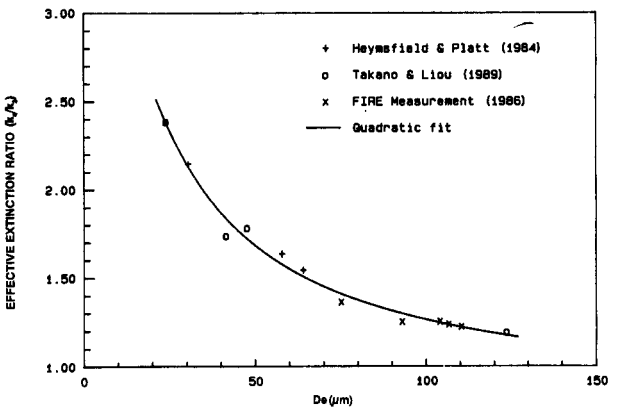

Fig. 1. Effective extinction ratio k_4/k_3 as a function of the mean effective size D_e. Points are based on a number of measured ice-crystal size distributions and the curve is the best quadratic fit.

squares fitting in terms of $1/D_e$ in the form

$$k_4/k_3 = \sum_{n=0}^{2} b_n D_e^{-n}, \tag{8}$$

where $b_0 = 0.722$, $b_1 = 55.08$, and $b_2 = -174.12$. The fitted curve is also shown in the figure. The root-mean-square difference between the computed and least-squares fitted values of k_4/k_3 is 0.045, which indicates that the polynomial fitting is an excellent parameterization to relate k_4/k_3 and D_e.

We have also carried out calculations of k_4 and k_3 by using area-equivalent ice spheres, which would give approximately the same extinction cross section as nonspherical ice crystals. If the number density and cloud thickness remain unchanged, then the cloud optical depth would be approximately the same for spherical and nonspherical ice particles. For the Cs case ($D_e \cong 41.5$ μm), the k_4/k_3 value is ~1.50 for ice spheres compared with a value of ~1.75 for hexagonal ice crystals. This difference can produce errors in the retrievals of cloud temperature by more than ~7 K. The difference for the k_4/k_3 values between spherical and nonspherical ice particles increases (decreases) as the mean effective size D_e decreases (increases).

A direct determination of D_e from data of satellite IR channels that are presently available appears to be difficult. However, we may relate D_e to the cloud temperature through appropriate observations. From a large number of cirrus microphysical data collected by optical probes during flights over midlatitudes, Heymsfield and Platt[14] have suggested that ice-crystal size distribution can be represented by a general power form,

$$n(L) = \begin{cases} A_1 L^{b1}(\text{IWC}), & L \le L_0 \\ A_2 L^{b2}(\text{IWC}), & L > L_0, \end{cases} \tag{9}$$

where $L_0 = (A_2/A_1)^{1/(b_1-b_2)}$; IWC is the ice-water content; and $A_{1,2}$ and $b_{1,2}$ are empirical coefficients determined from the measured data. The values of b, A, and IWC may be parameterized in terms of temperature in the range of −20° to −60°C.[18] Using this parameterization, we find that $n(L)$ is a function of temperature. Moreover, based on aircraft and laboratory measurements, the width D and the length L are related (see, e.g., Auer and Veal[19]) in such a way that a parameterization relation can be developed for the two. Thus, with the functional form of $n(L)$ determined, the mean effective size D_e can be obtained from Eq. (7). Subsequently we perform a least-squares polynomial fitting to relate D_e to T_c, in the form

$$D_e = \sum_{n=0}^{3} c_n (T_c - 273)^n, \tag{10}$$

where $c_0 = 326.3$, $c_1 = 12.42$, $c_2 = 0.197$, and $c_3 = 0.0012$.

Finally, in order to solve Eq. (6) for $B_4(T_c)$, the upwelling radiances reaching the cloud base, $R_{a3,4}$, must be given. We may approximate these radiances by radiances measured from satellites in clear conditions because little water vapor is present above cirrus clouds. In the case of AVHRR data, each scan line spans ~2500 km. Because of the high resolution of the AVHRR data points, it is most likely that, over a large area scanned by the radiometer, some of the data points correspond to clear conditions. It follows that if we can identify the clear data points, $R_{a3,4}$ may be determined by a statistical method. We may select a scene and use the data within this scene to construct a two-dimensional histogram in the domain of R_3 and R_4. The area of the scene should be large enough to contain a statistically significant amount of data points, but, at the same time, this area should also be sufficiently small to guarantee the homogeneity of the surface temperature and water-vapor distributions within the scene. Usually, a 1° by 1° scene is adequate for the analysis. The radiances corresponding to the peak of the frequency distribution are assigned as the mean clear radiances. Details for the determination of clear radiances are illustrated in Section 4.

3. Sensitivity Studies

In order to apply the above algorithm for the inference of cloud parameters, we must first determine whether cirrus clouds are present within the field of view of the radiometers. We have investigated the information content of the BTD between Ch. 3 and Ch. 4 radiances. The brightness temperature is defined as the equivalent blackbody temperature that corresponds to the measured radiance and is determined through the Planck function. First we carry out an analysis concerning the sensitivity of BTD values to various cloudy conditions. For optically thick clouds, the upwelling radiances for the two channels are approximately equal to the Planck intensities; a result that can be obtained from expressions (1) for $\epsilon_{3,4} = 1.0$. The plot of the Planck intensities by Eq. (2) over the range of cloud temperature T_c is shown in Fig. 2 as the solid curve. This curve is the limiting case, which corresponds to perfect blackbody

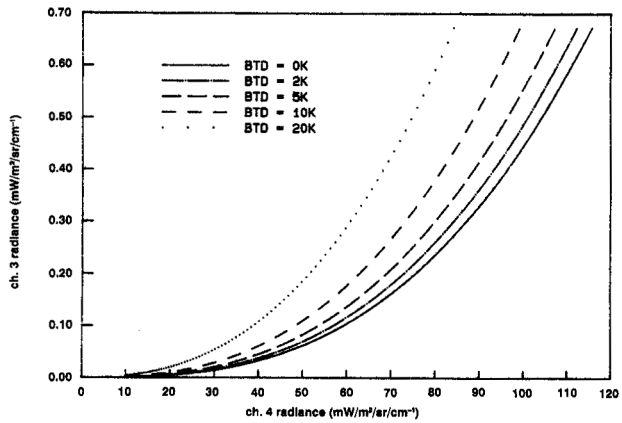

Fig. 2. Constant BTD lines for BTD = 0, 2, 5, 10, and 20 K in the domain of Ch. 3 and Ch. 4 radiances.

emission. The radiances can be converted to the brightness temperatures through the Planck function along the curve BTD = 0.0. For nonblack cirrus clouds, $\epsilon < 1.0$, the brightness temperature of Ch. 3 is larger than that of Ch. 4. The reason for this behavior is as follows. First, $\epsilon(3.7\ \mu m)$ is usually less than $\epsilon(10.9\ \mu m)$. As a result, the 3.7-μm transmittance is larger than the 10.9-μm transmittance, which implies a larger transmission of below-cloud radiance for the former wavelength. Second, the temperature dependence of the Planck function at 3.7 μm is approximately three times larger than that at 10.9 μm. Thus, in the retrieval analysis, we may determine cirrus pixels by filtering out those pixels with a BTD that is less than a threshold value. In the case in which the cloud optical properties are similar (e.g., at large D_e, $k_4 \cong k_3$), differential brightness temperatures for $\epsilon < 1.0$ are produced by the Planck function at two different wavelengths; the degree of the differences depends on the cloud position and cloud composition. Figure 2 also shows the contours for BTD = 2, 5, 10, and 20 K. These curves are obtained from the look-up table described in Section 2. From simulation results that are discussed below, we find that data points corresponding to cirrus conditions generally have a BTD larger than 2 K. As shown in Section 4, the BTD's from the measured satellite radiances over cirrus clouds are also larger than 2 K.

Next we investigate the sensitivity of upwelling radiances to cloud base height. We have selected the midlatitude summer profile[20] for the study. The bases of cirrus clouds are prescribed at 7, 9, and 11 km. For each cirrus height, we use 11 visible optical depths, ranging between 0.4 and 9, and compute their corresponding emissivity values according to Eqs. (3). Upwelling radiances from cirrus atmospheres are computed from expressions (1). The ratio k_4/k_3 is fixed as 1.07, which corresponds to $D_e \sim 200\ \mu m$. Figure 3 shows the distributions of Ch. 3 and Ch. 4 radiances, along with the Planck intensity curve [Eq. (2)]. The simulated cloud-base radiances are 0.45 and 100 mW/m^2/sr/cm^{-1} for Chs. 3 and 4, respectively. The Planck intensities of surface temperature (294 K) are 0.48 and 102.4 mW/m^2/sr/cm^{-1}, respectively. The simulated clear radiances are close to, but not exactly the same as, the corresponding surface Planck intensities, because of the effects of small water-vapor absorption. From Eq. (5) we find that radiances for the same cirrus base height form a curve that is nearly linear because k_4/k_3 is close to 1. As the cloud base height increases, both radiances for the same optical depth decrease. The radiance curve for the same height intercepts the Planck intensity curve at lower radiance values. The radiances at the intercept ($\epsilon \to 1$) correspond to the Planck intensities of cirrus temperature according to expressions (1). Similar patterns also occur in the study that uses tropical atmospheric profile.[20]

Moreover we study the effects of k_4/k_3 on the cloud temperature retrieval. Figure 4 shows the curves of R_3 versus R_4 for three different values of k_4/k_3 that are based on Eq. (5). The cirrus height is fixed at 9 km. As shown in this diagram, the Ch. 3 radiances are sensitive to the value of k_4/k_3. A variation in k_4/k_3 from 1 to 3 leads to the maximum change in Ch. 3 radiances of ~ 0.2 mW/m^2/sr/cm^{-1}. The Ch. 4 radiances are nearly independent of k_4/k_3 because k_4 changes little over the range of D_e considered here. An incorrect value of k_4/k_3 can produce significant errors in the retrieved cloud temperature and optical depth. As an example, let Ch. 3 and Ch. 4 radiances be 0.26 and 70 mW/m^2/sr/cm^{-1}, respectively. If we prescribe k_4/k_3 with a value of 1, the retrieved cloud temperature and optical depth will be ~ 240 K and 1.3, respectively. However, if we set k_4/k_3 to a value of 3, then the cloud temperature and optical depth will differ by ~ 30 K and 4.2, respectively. The differences represent an extreme case. Nevertheless this example does point out the importance of incorporating the dependency of k_4/k_3 on D_e in the retrieval analysis. By comparing Fig. 2 with Figs. 3 and 4, we clearly see that BTD values are the observed quanti-

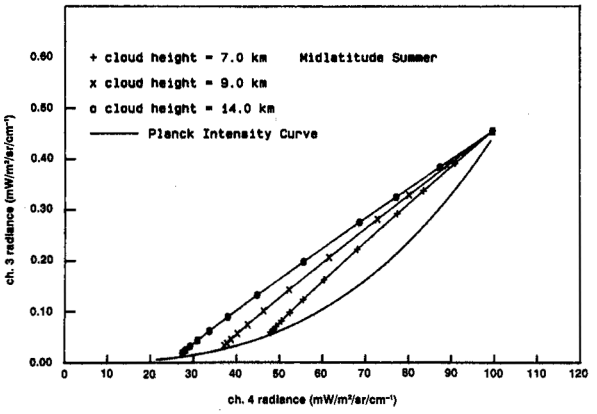

Fig. 3. Distributions of the computed Ch. 3 and Ch. 4 radiances that are based on expressions (1) along with the Planck intensity curve. The clear radiances are obtained from the midlatitude summer profile. Cloud bases are set at 7, 9, and 11 km. The ratio k_4/k_3 is fixed at a value of 1.07.

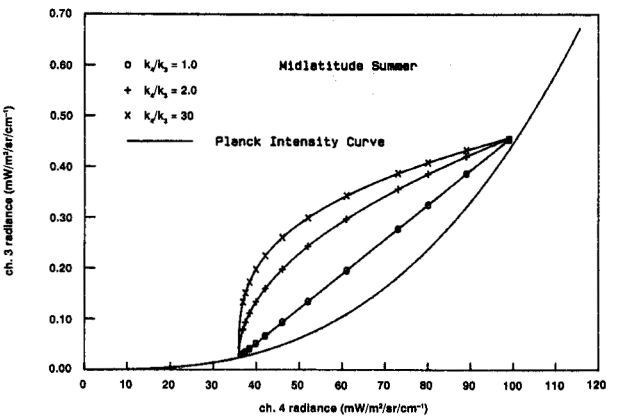

Fig. 4. Distributions of the computed Ch. 3 and Ch. 4 radiances that are based on Eq. (6) for three values of k_4/k_3. The cloud height is 9 km. Also shown is the Planck intensity curve.

ties that can be used to identify the presence of cirrus clouds.

Once the cirrus pixels are identified and clear column radiances are determined, iterative procedures are established to solve for T_c, $\epsilon_{3,4}$, and D_e simultaneously. Figure 5 shows a schematic description of the sequence of iterations. Equation (6) is solved by using a modified Newton's iteration scheme, which is efficient for the solution of nonlinear algebraic equations.

Finally, we examine the potential instrument noises for Chs. 3 and 4 on the above retrieval method. According to Dudhia,[21] the noises in terms of the brightness temperature are of the order of 0.4 and 0.03 K for Ch. 3 and Ch. 4, respectively. These values have been obtained from measurements from AVHRR IR channels on NOAA-9 and NOAA-10 satellites. The noise for Ch. 3 exceeds the design specification of 0.12 K. Random numbers within the uncertainty range are generated and added to the brightness temperatures associated with R_{ai} and R_i, which are then converted to radiances. Subsequently we perform retrievals by using perturbed radiances. The results indicate that the errors of retrieved temperatures increase with the cirrus cloud height, but decrease with increasing emissivity. The largest maximum errors are less than ~ 2 K. Errors in cloud temperature are largely independent of the temperature profile. In general, for $\epsilon > 0.5$, the error is less than 0.5 K. The errors in the retrieved emissivities are less than 0.1%.

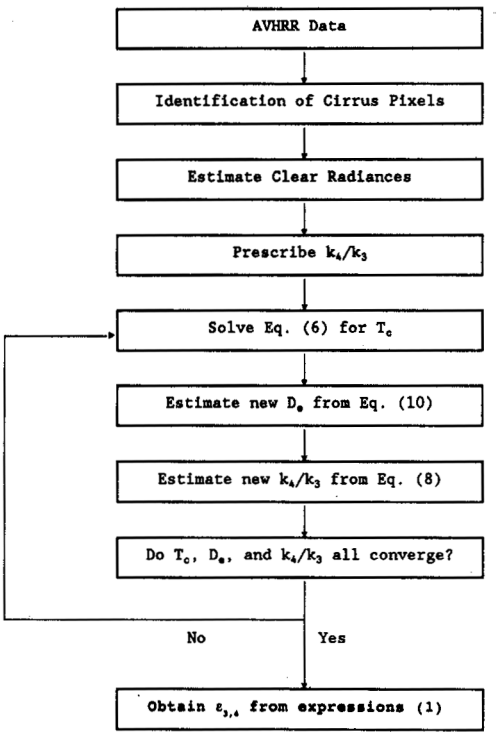

Fig. 5. Schematic description of the iterative procedures for the simultaneous solution of cloud temperature, cloud emissivities, and mean effective size.

4. Application to FIRE-IFO Data

For the purpose of testing the retrieval scheme, we have acquired the AVHRR GAC (global area coverage) data collected at 0930 UTC (local nighttime), 28 October 1986, over the FIRE-IFO region (42°–47° N; 87°–92° W). The resolution near the satellite nadir is 1 km × 4 km, and all IR channel data have been converted to brightness temperatures. Figures 6(a), 6(b), and 6(c) show the halftone display for the brightness temperatures of Ch. 3 and Ch. 4, and the associated BTD map, respectively. Several pockets of cold brightness temperature are shown in the upper-left quadrant. These areas are cloudy. However, it is not clear from the displays presented in Figs. 6(a) and 6(b) whether the clouds are cirrus or water clouds. Figure 6(c) shows that the BTD's over these cloudy areas largely exceed 4 K. According to the discussion in Section 3, these cloudy pockets must be cirrus clouds.

To test the present retrieval algorithm, we focus on a region west of Fort McCoy (43.9° N; 90.8° W; marked as x in Figs. 6). We select the data for a zone from 43.5° to 44.5° N and from 91° to 92° W (highlighted in Fig. 6) that consists of a total of 668 satellite data points. Within this zone, a band of cirrus extends from the northwest to the southeast. This region was selected because the air mass over this region drifted over Fort McCoy approximately two hours later (see below for further discussion), when surface lidar observations became available. Also, the distinctive feature of the cirrus cloud band and the well-defined clear area made it suitable for testing the current retrieval scheme.

Figure 7 shows a three-dimensional display of the frequency distribution of the radiance pair R_3, R_4, which is based on the AVHRR data set. The maximum frequency radiance values are $R_3 = 0.21$ and $R_4 = 78$ mW/m^2/sr/cm^{-1}, which correspond to clear conditions. These values are asssigned as the mean clear radiances. The spread of clear radiances is presumably due to the nonhomogeneity of the land surface temperature or the surface emissivity of Ch.3. We have investigated the effects of area selection on the determination of clear radiances by reducing the area of interest to a zone from 44.0° to 44.5° N and from 91.5° to 92.0° W. This reduced area contains a major part of the cirrus band. All the pixels that contain cirrus data are largely preserved. The variability in clear radiances is much reduced. However, the mean clear radiances remain unchanged. We have also compared the clear brightness temperatures that are converted from radiances with the surface temperature (~ 278 K) reported from the sounding. Differences are less than 1 K. We have set a clear BTD threshold value of ~ 2 K to differentiate between clear and cloudy conditions. A total of 580 clear pixels are identified, as described in Section 3. The remaining 88 data points are classified as cirrus clouds.

To estimate the range of cloud parameters before carrying out retrieval, we show a two-dimensional

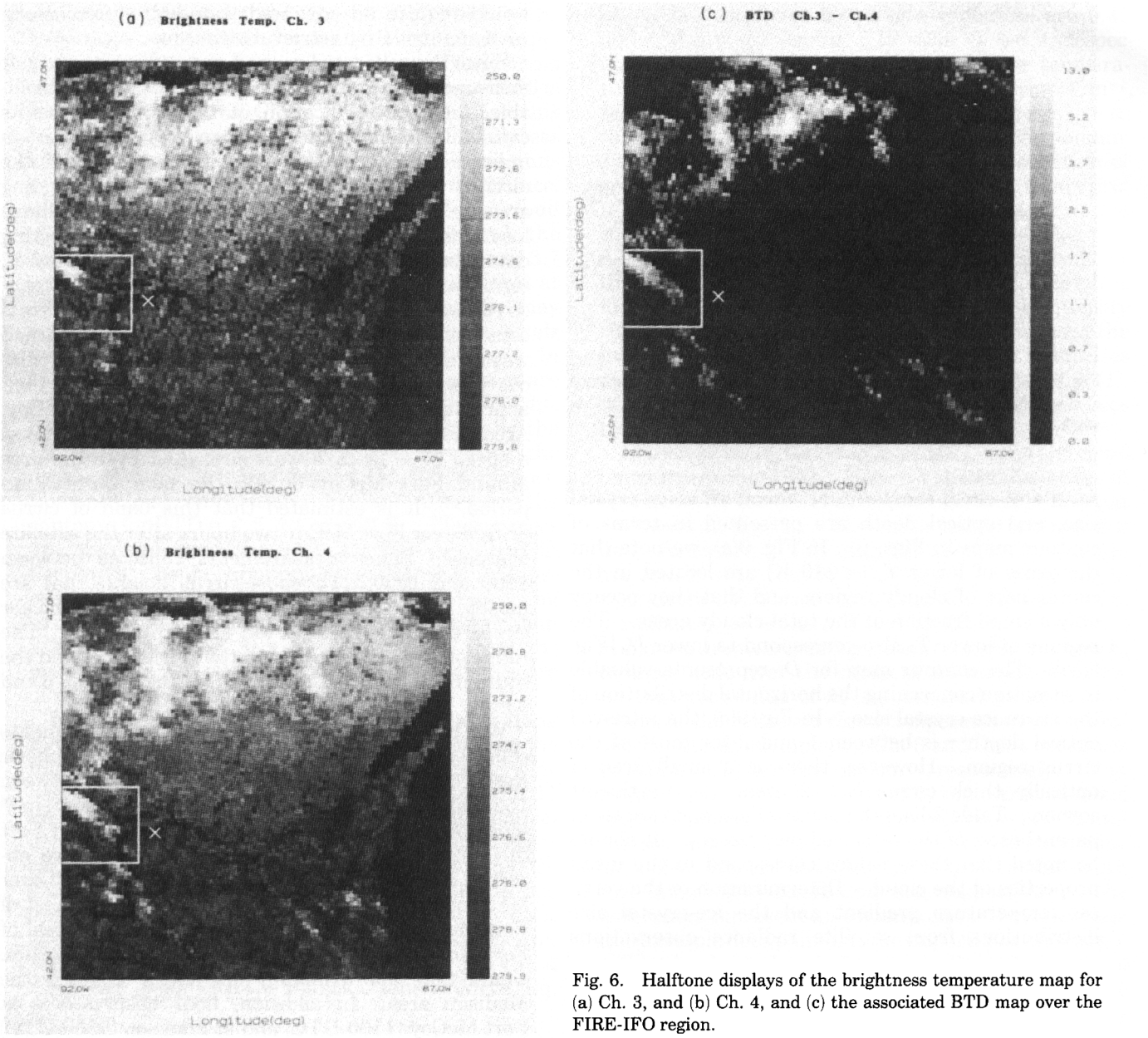

Fig. 6. Halftone displays of the brightness temperature map for (a) Ch. 3, and (b) Ch. 4, and (c) the associated BTD map over the FIRE-IFO region.

display of R_3 versus R_4 for data points that have been identified as cirrus clouds (Fig. 8). This analysis is helpful in prescribing the initial cloud parameters for numerical iteration and for checking the reliability of the retrieved values. The cross symbol depicted at the upper right denotes the mean clear radiances determined from satellite data. Superimposed on these data points are the three theoretical curves for k_4/k_3 = 1.8, 1.4, and 1.1, according to Eq. (5), in which three cloud temperatures of 220, 235, and 250 K are used in the calculations. The corresponding values for D_e from Eq. (10) are 45, 70, and 150 μm. These three curves show the combined effects of ice-crystal size and cloud height. For lower cirrus clouds and larger ice crystals, the theoretical curve is closer to the Planck intensity curve. It is evident that a major portion of data points lies between the curves corresponding to k_4/k_3 of 1.4 and 1.1. Accordingly, for these data points, the cloud temperature T_c should be between 235 and 250 K, while the mean effective size D_e should be between 70 and 150 μm. In addition, when expressions (1) and Eq. (5) are used, the 10.9-μm emissivity should range between 0.2 and 0.7. From the temperature sounding report of Fort McCoy at 0900 UTC, we estimate that the range of cirrus heights (z_c is between 6 and 9 km.

The retrieval program is applied to each satellite data point that has been identified as cirrus. To guarantee the numerical stability in the retrieval, we rejected 18 pairs of R_3, R_4 involving a 10% difference between either R_3 and R_{a3} or between R_4 and R_{a4}.[7] This is because uncertainities that are due to the spread of clear radiances can result in unrealistic values for the retrieved cirrus parameters. The

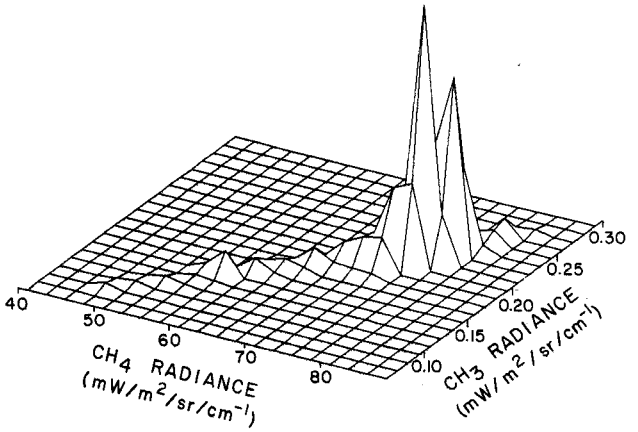

Fig. 7. Three-dimensional display of the frequency of occurrence of the radiance pair R_3, R_4 based on the AVHRR data used in this work.

results of cloud temperature, mean effective crystal size, and optical depth are presented in terms of contour maps in Figs. 9. In Fig. 9(a), we note that the areas of lower T_c (<240 K) are located in the center part of cloudy regions and that they occupy only a small fraction of the total cloudy areas. The regions of lower T_c also correspond to lower D_e [Fig. 9(b)]. The contour map for D_e represents valuable information concerning the horizontal distribution of the mean ice-crystal size. In Fig. 9(c), the retrieved optical depth τ is between 1 and 2 for most of the cirrus region. However, there is a small area of optically thick cirrus ($\tau > 2$) near the northwest corner. Table 2 lists the mean values and ranges (in parentheses) of the retrieved parameters. It should be noted that these values correspond to the mean properties of the cloud. Determination of the vertical temperature gradient and the ice-crystal size distributions from satellite radiance observations

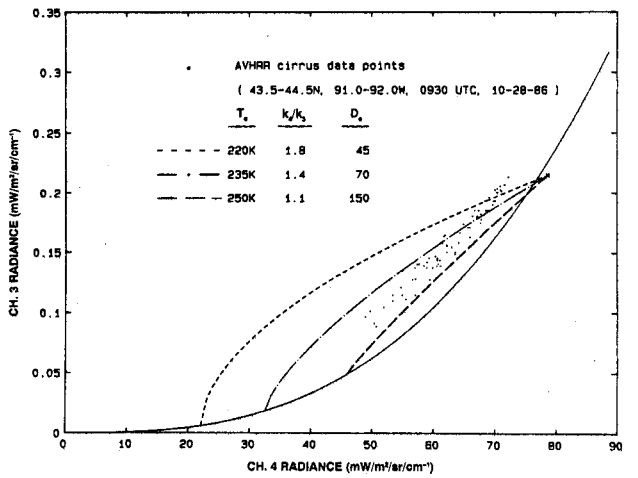

Fig. 8. Two-dimensional display of AVHRR Ch. 3 and Ch. 4 radiances for data points that have been identified as cirrus. The cross symbol denotes the mean clear radiances determined from satellite data. Superimposed on these data points are the theoretical curves for $k_4/k_3 = 1.8$, 1.4, and 1.1, according to Eq. (5).

would require an advanced sounding system along with an innovative retrieval technique.

Since the collocated ground and the *in situ* aircraft measurements for cloud parameters are not available, a direct verification of the retrieved results cannot be made. However, we may carry out an indirect comparison by using the surface and the aircraft data that are available in the surrounding areas. The Langley Research Center lidar systems located at Fort McCoy were continuously collecting data from 0800–2400 UTC, 28 October. However, significant responses that were due to the presence of cirrus were detected only after 1100 UTC.[22] This is consistent with satellite observations because there was no cirrus over Fort McCoy at the time of satellite overpass (0930 UTC). The cirrus band was then approximately 50 to 100 km west of Fort McCoy. According to the synoptic analysis, northwesterlies at a speed of ~ 15 m/s were prevalent over the area around Fort McCoy during the lidar observation period.[23] It is estimated that this band of cirrus drifted over Fort McCoy two hours after the satellite overpass. Lidar measurements collected between 1100 and 1500 UTC show cirrus heights that are mostly between 6 and 8 km. Higher and thicker cirrus clouds were observed after 1500 UTC. The range of height derived from the retrieved T_c and the sounding at Fort McCoy (0900 UTC) is between 6 and 9 km.

We have acquired microphysical measurements collected by the National Center for Atmospheric Research King Air turboprop on 28 October, between 1525 and 1729 UTC, near Madison, Wisconsin.[24] Madison is approximately 250 km southeast of Fort McCoy. From the satellite cloud pictures, we observed that the cirrus that the aircraft observed over Madison drifted from the cloud band located west of Fort McCoy. We estimate that the air mass west of Fort McCoy, driven by the prevalent northwesterlies, would take approximately six hours to reach the Madison area. In addition, lidar observations at Fort McCoy (1100 UTC) and at Madison (1500 UTC) both recorded cirrus cloud heights of between 6 and 9 km. The aircraft was equipped with two Particle Measuring systems two-dimensional (2D) probes for the detection of ice particles. The 2D C probe measures the size of ice crystals from 25 μm to ~ 1 mm in 25-μm increments. The two-dimensional P probe measures ice crystals with dimensions ranging between 100 μm and ~ 2 mm in 100-μm increments. Samplings were taken every 5 s. A composite size distribution was derived for each sampling from the combined 2D probe data by using a scheme that emphasized the best measurement range of each instrument. We used the average composite size distributions of all samplings taken during the 2-h flight period to derive a mean D_e of ~ 107 μm, based on Eq. (10). This value is close to the mean D_e (~ 104 μm) retrieved from satellite data. The average composite size distribution for this particular case exhibits the two-section power form described in

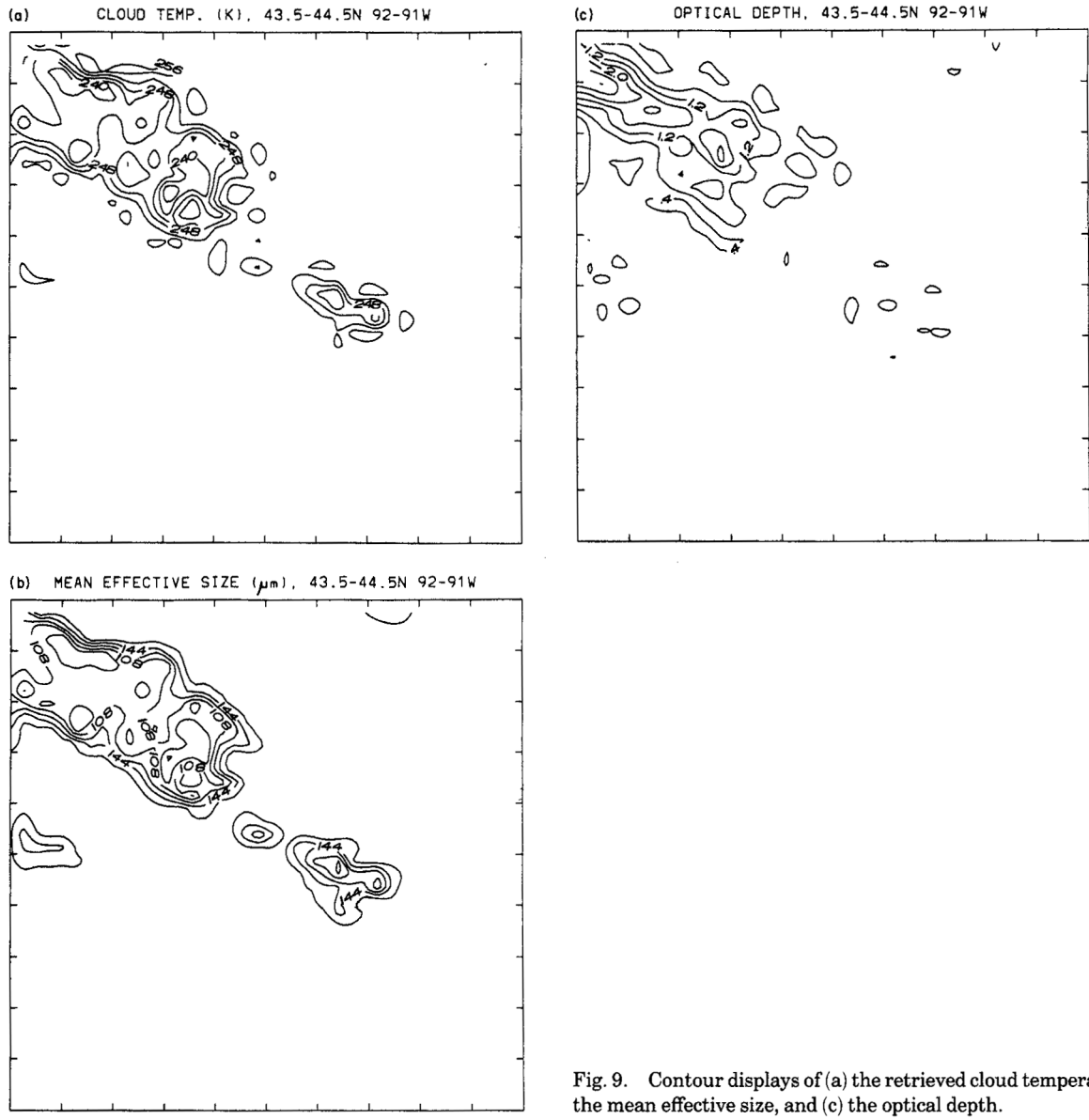

Fig. 9. Contour displays of (a) the retrieved cloud temperature, (b) the mean effective size, and (c) the optical depth.

Eq. (9), which is common for cirrus clouds with temperatures greater than −40°C. The values for slopes b_1 and b_2 are approximately −2.0 and −6.0, respectively, while the coefficients A_1 and A_2 are 1.403×10^8 and 9.36×10^{18}, respectively. The values that were used to obtain k_4/k_3 are $b_1 = -2.27$, $b_2 = -5.87$, $A_1 = 2.58 \times 10^8$, and $A_2 = -5.58 \times 10^{18}$; these values are based on the results presented by Heymsfield and Platt.[14] The two sets of data for the determination of ice-crystal size distribution are fairly close.

Table 2. Mean Values of the Retrieved Parameters for Cirrus Pixels within a 1° × 1° Scene West of Fort McCoy at 0930 UTC, 28 October 1986

Parameter	Current Scheme
T_c (K)	244 (233–255)
ϵ_3	0.36 (0.17–0.70)
ϵ_4	0.42 (0.20–0.76)
τ	1.08 (0.41–2.77)
k_4/k_3	1.25 (1.07–1.44)
D_e (μm)	104 (68–156)
z_c (km)	7.5 (6–9)[a]

[a]Inferred from the Fort McCoy sounding at 0900 UTC.

5. Conclusions

The current retrieval scheme uses radiance data of AVHRR IR channels to determine cirrus temperature, mean effective size, and optical depth simultaneously from the theory of radiative transfer. We have focused our efforts on the retrieval of cirrus parameters by using AVHRR Ch. 3 (3.7-μm) and Ch. 4 (10.9-μm) radiances. These channels are affected relatively little by the presence of water vapor and are, therefore, ideal for the inference of cirrus cloud parameters.

In order to solve the governing equations, we have established relationships between the emissivities of the two channels and have introduced a parameter

k_4/k_3, which is a function of ice-crystal size distribution. Using a number of typical size distribution functions taken from the data presented by a number of researchers, we have examined the dependence of k_4/k_3 on the mean effective size that defines ice-crystal size distribution. The value k_4/k_3 decreases as the mean effective size increases. We have developed a parameterization of k_4/k_3 in terms of mean effective size.

We have performed sensitivity studies on the effects of cirrus parameters on upwelling radiances. We find that for higher cirrus and smaller cirrus particle size, the brightness temperature difference becomes larger, and that nonzero BTD's between the two channels are good indicators of the presence of cirrus clouds. In addition, we show that radiances from cirrus cloudy atmospheres depend significantly on k_4/k_3 and that variations in k_4/k_3 must be accounted for in the retrieval.

Finally, the current retrieval scheme has been applied to satellite data collected over the FIRE-IFO region. The retrieved cirrus heights are in general agreement with lidar observations at Fort McCoy two hours after a satellite overpass. The retrieved mean effective size is close to that derived from *in situ* aircraft microphysical measurements over Madison six hours after a satellite overpass.

This work was supported by the Small Business Innovation Research Program under contract F19628-90-C-0123, Geophysics Directorate of the Phillips Laboratory, U.S. Air Force, Bedford, Mass. Thanks are due to P. Minnis of NASA Langley Research Laboratory, Langley, Va., for providing the AVHRR GAC data on the FIRE-IFO region and to J. W. Snow and his colleagues at the Satellite Meterology Branch of the Geophysics Directorate for offering helpful comments on this paper. Kathy Roberts and Jennifer Bangerter typed the manuscript.

References

1. K. N. Liou, "Influence of cirrus clouds on weather and climate processes: a global perspective," Mon. Weather Rev. **114,** 1167–1199 (1986).
2. K. N. Liou, "Remote sensing of the thickness and composition of cirrus clouds from satellites," J. Appl. Meteorol. **16,** 91–99 (1977).
3. G. Szejwach, "Determination of semi-transparent cirrus cloud temperature from infrared radiances: application to METEOSAT," J. Appl. Meteorol. **21,** 384–393 (1982).
4. W. Pollinger and P. Wendling, "A bispectral method for the height determination of optically thin ice clouds," Contrib. Atmos. Phys. **57,** 269–281 (1984).
5. R. Huang and K. N. Liou, "Remote sounding of cirrus optical depth and temperature from 3.7 and 11 micrometer windows," Adv. Atmos. Sci. **1,** 150–164 (1984).
6. A. Arking and J. D. Childs, "Retrieval of cloud cover parameters from multispectral satellite images," J. Clim. Appl. Meteorol. **23,** 322–333 (1985).
7. K. N. Liou, S. C. Ou, Y. Takano, F. P. J. Valero, and T. P. Ackerman, "Remote sounding of the tropical cirrus cloud temperature and optical depth using 6.5 and 10.5 μm radiometers during STEP," J. Appl. Meteorol. **29,** 716–726 (1990).
8. S. A. Ackerman and W. L. Smith, "Inferring cloud microphysical properties from high resolution spectral measurements in the 8-13 μm window region," in *Preprints of the Seventh Conference on Atmospheric Radiation* (American Meteorological Society, Boston, Mass., 1990), pp. 6–8.
9. S. Kinne, T. Ackerman, A. Heymsfield, and K. Miller, "Radiative transfer in cirrus clouds from airborne flux and microphysical measurements during FIRE 86," in *Preprints of the Seventh Conference on Atmospheric Radiation* (American Meteorological Society, Boston, Mass., 1990), pp. 9–15.
10. T. Inoue, "On the temperature and effective emissivity determination of semi-transparent cirrus clouds by bi-spectral measurements in the 10 μm window region," J. Meteorol. Soc. Jpn. **63,** 88–98 (1985).
11. M. L. Wu, "A method for remote sensing the emissivity, fractional cloud cover and cloud top temperature of high level, thin clouds," J. Clim. Appl. Meteorol. **26,** 225–233 (1987).
12. R. P. d'Entremont, M. K. Griffin, and J. T. Bunting, "Retrieval of cirrus radiative properties and altitudes using multichannel infrared data," in *Preprint of the AMS Fifth Conference on Satellite Meteorology and Oceanography* (American Meteorological Society, Boston, Mass., 1990), pp. 4–9.
13. R. S. Stone, G. L. Stephens, C. M. R. Platt, and S. Banks, "The remote sensing of thin cirrus cloud using satellites, lidar and radiative transfer theory," J. Appl. Meteorol. **29,** 353–366 (1990).
14. A. J. Heymsfield and C. M. R. Platt, "A parameterization of the particle size spectrum of ice clouds in terms of the ambient temperature and the ice water content," J. Atmos. Sci. **41,** 846–855 (1984).
15. Y. Takano and K. N. Liou, "Solar radiative transfer in cirrus clouds. Part I: Single-scattering and optical properties of hexagonal ice crystals," J. Atmos. Sci. **46,** 3–19 (1989).
16. Y. Takano and K. N. Liou, "Solar radiative transfer in cirrus clouds. Part II: Theory and computation of multiple scattering in an anisotropic medium," J. Atmos. Sci. **46,** 20–36 (1989).
17. K. N. Liou, Y. Takano, S. C. Ou, A. Heymsfield, and W. Kreiss, "Infrared transmission through cirrus clouds: a radiative model for target detection," Appl. Opt. **29,** 1886–1896 (1990).
18. K. N. Liou, *Radiation and Cloud Processes in the Atmosphere: Theory, Observation and Modelling* (Oxford U. Press, Oxford, 1992).
19. A. H. Auer and D. L. Veal, "The dimension of ice crystals in natural clouds," J. Atmos. Sci. **27,** 919–926 (1970).
20. R. A. McClatchey, R. W. Fenn, J. E. A. Selby, F. E. Volz, and J. S. Garing, "Optical properties in the atmosphere," Environmental Research Paper No. 354, AFCRL-71-0279, AD726116, (U.S. Government Printing Office, Washington, D.C., 1971).
21. A. Dudhia, "Noise characteristics of the AVHRR infrared channels," Int. J. Remote Sensing **10,** 637–644 (1989).
22. K. Sassen, C. J. Grund, J. D. Spinhirne, M. M. Hardesty, and J. M. Alvarez, "The 27–28 October 1986 FIRE IFO cirrus case study: a five lidar overview of cloud structure and evolution," Mon. Weather Rev. **118,** 2288–2311 (1990).
23. D. O'C. Starr and D. P. Wylie, "The 27–28 October 1986 FIRE cirrus case study: meteorology and clouds," Mon. Weather Rev. **118,** 2259–2287 (1990).
24. A. J. Heymsfield, K. M. Miller, and J. D. Spinhirne, "The 27–28 October 1986 FIRE IFO cirrus case study: cloud microstructure," Mon. Weather Rev. **118,** 2313–2328 (1990).